J|A|C|S
ARTICLES
Published on Web 11/27/2003

Solventless Synthesis of Monodisperse Cu_2S Nanorods, Nanodisks, and Nanoplatelets

Michael B. Sigman, Jr., Ali Ghezelbash, Tobias Hanrath, Aaron E. Saunders, Frank Lee, and Brian A. Korgel*

Contribution from the Department of Chemical Engineering, Texas Materials Institute, Center for Nano- and Molecular Science and Technology, The University of Texas at Austin, Austin, Texas 78712-1062

Received July 31, 2003; E-mail: korgel@che.utexas.edu

Abstract: Cu_2S nanocrystals with disklike morphologies were synthesized by the solventless thermolysis of a copper alkylthiolate molecular precursor. The nanodisks ranged from circular to hexagonal prisms from 3 to 150 nm in diameter and 3 to 12 nm in thickness depending on the growth conditions. High resolution transmission electron microscopy (HRTEM) revealed the high chalcocite (hexagonal) crystal structure oriented with the *c*-axis ([001] direction) orthogonal to the favored growth direction. This disk morphology is thermodynamically favored as it allows the extension of the higher energy {100} and {110} surfaces with respect to the {001} planes. The hexagonal prism morphology also appears to relate to increased C−S bond cleavage of adsorbed dodecanethiol along the more energetic {100} facets relative to {001} facets. Monodisperse Cu_2S nanodisks self-assemble into ribbons of stacked platelets. This solventless approach provides a new technique to synthesize anisotropic metal chalcogenide nanostructures with shapes that depend on both the face-sensitive thermodynamic surface energy and the surface reactivity.

Introduction

The physical properties of inorganic nanostructures fundamentally relate to their chemical composition, size, crystal structure, surface chemistry, and shape. The ability to synthetically tune these material parameters provides the opportunity to study and understand the relationship between chemical, structural, and quantum effects that occur uniquely at the nanoscale. Solution-phase synthetic approaches have been applied with a high degree of success to produce a variety of different nanocrystal materials, with very controllable size and size distributions in many cases.[1] Due to the importance of dimensionality on the properties of nanoscale materials, there has been a significant effort in identifying routes to controlling shape using these colloidal synthetic methods. In these methods, inorganic particles are controllably precipitated from molecular precursors in the presence of organic ligands. The ligands adsorb to the nanocrystal surface and control growth by providing steric stabilization and preventing aggregation. The adsorbed ligands can change the growth kinetics and surface energies of different crystal faces, which can ultimately lead to anisotropic growth of low symmetry nanostructures, such as nanorods, nanodisks, and nanowires.[2,3] The internal crystallinity also influences the nanocrystal shape, as different crystal planes exhibit significantly different surface energies: even nanocrystals with "spherical" morphologies typically exhibit facetted geometries such as truncated icosahedrons that reduce exposure of high energy crystal planes.[4] Materials with anisotropic crystal structure, such as hexagonal materials, are particularly predisposed to anisotropic growth, as the {001} planes (those perpendicular to the *c*-axis) exhibit significantly different surface energies relative to the {100} and {110} crystal planes. Nanocrystals with aspherical structures including cubes, rods, platelets, and wires have been formed from a variety of materials such as Ag,[5] Au,[5,6] $BaWO_4$,[7] CdSe,[3] Co,[2] Cu,[8] GaN,[9] GaP,[10] InP,[11] Ni,[12] NiO,[13] Se,[14] and Si.[15]

We recently synthesized Cu_2S nanorods by the solventless thermolysis of a molecular copper alkylthiolate precursor.[16] Nanorods with very monodisperse size and shape can be produced using this method, and strands of self-assembled nanorods can be formed that extend micrometers in length. We have since synthesized Cu_2S nanostructures by this technique

(1) Murray, C. B.; Kagan, C. R.; Bawendi, M. G. *Annu. Rev. Mater. Sci.* **2000**, *30*, 545.
(2) Puntes, V. F.; Zanchet, D.; Erdonmez, C. K.; Alivisatos, A. P. *J. Am. Chem. Soc.* **2002**, *124*, 12874.
(3) Peng, X.; Manna, L.; Yang, W.; Wickham, J.; Scher, E.; Kadavanich, A.; Alivisatos, A. P. *Nature* **2000**, *404*, 59.
(4) Korgel, B. A.; Fullam, S.; Connolly, S.; Fitzmaurice, D. *J. Phys. Chem. B* **1998**, *102*, 8379.
(5) Sun, Y.; Xia, Y. *Science* **2002**, *298*, 2176.
(6) Nikoobakht, B.; El-Sayed, M. A. *Chem. Mater.* **2003**, *15*, 1957.
(7) Kwan, S.; Kim, F.; Akana, J.; Yang, P. *Chem. Commun.* **2001**, *5*, 447.
(8) Liu, Z.; Bando, Y. *Adv. Mater.* **2003**, *15*, 303.
(9) Bae, S. Y.; Seo, H. W.; Park, J.; Yang, H.; Kim, H.; Kim, S. *Appl. Phys. Lett.* **2003**, *82*, 4564.
(10) Kim, Y.-H.; Jun, Y.-w.; Jun, B.-H.; Lee, S.-M.; Cheon, J. *J. Am. Chem. Soc.* **2002**, *124*, 13656.
(11) Ahrenkiel, S. P.; Micic, O. I.; Miedaner, A.; Curtis, C. J.; Nedeljkovic, J. M.; Nozik, A. J. *Nano Lett.* **2003**, *3*, 833.
(12) Cordente, N.; Respaud, M.; Senocq, F.; Casanove, M.-J.; Amiens, C.; Chaudret, B. *Nano Lett.* **2001**, *1*, 565.
(13) Wang, W.; Liu, Y.; Xu, C.; Zheng, C.; Wang, G. *Chem. Phys. Lett.* **2002**, *362*, 119.
(14) Gates, B.; Mayers, B.; Cattle, B.; Xia, Y. *Adv. Funct. Mater.* **2002**, *12*, 219.
(15) Holmes, J. D.; Johnston, K. P.; Doty, R. C.; Korgel, B. A. *Science* **2000**, *287*, 1471.
(16) Larsen, T. H.; Sigman, M.; Ghezelbash, A.; Doty, R. C.; Korgel, B. A. *J. Am. Chem. Soc.* **2003**, *125*, 5638.

10.1021/ja037688a CCC: $25.00

over a wider range of reaction conditions than those previously reported and have found that the rods evolve into faceted platelets at larger sizes with the *c*-axis orthogonal to the growth axis. In fact, the smaller nanorods (4 nm × 12 nm) reported in ref 16 are more accurately described as platelets elongated along two axes; the platelets are oriented on end and therefore appear to be rodlike in the two-dimensional TEM images. This crystallographic orientation is unlike the majority of nanorod materials reported to date where growth is favored along the *c*-axis.[3,6,10,11,14] The hcp-Co nanodisks in ref 2 provide a notable exception to those cases. The Cu_2S nanodisks evolve into faceted platelets as a result of limited growth in the [001] direction. In this paper, we elucidate the growth mechanism and the underlying factors that determine the morphology of Cu_2S nanodisks formed by the solventless thermolysis of copper alkylthiolate and report the combined importance of face-sensitive surface energy and *reactivity* on the nanostructure morphology.

Materials and Methods

All chemicals were used as supplied from Aldrich Chemical Co. Water was doubly distilled and deionized. Cu_2S nanocrystals were obtained by the thermolysis of a copper-thiolate-derived precursor as described in ref 16. In a typical preparation, 32 mL of an aqueous copper(II) nitrate solution (0.21 g $Cu(NO_3)_2{\cdot}xH_2O$) are combined with 25 mL of $CHCl_3$ containing 0.08 to 0.21 g of sodium octanoate ($NaOOC(CH_2)_6CH_3$) to form a two-phase solution with a clear aqueous phase and a blue organic phase. The sodium octanoate serves as a phase transfer catalyst for the Cu^{2+} ions. After 20 min of vigorous stirring, the aqueous phase appears clear, at which point 240 μL of dodecanethiol ($C_{12}H_{25}SH$) are added. The organic phase changes color to a hue that ranges from blue-green to pale yellow depending on the initial amount of sodium octanoate used. After stirring for 10 min, the aqueous phase is discarded. The organic solvent is then evaporated to give a waxy solid. The waxy solid precursor material is heated in air for times ranging from 10 to 180 min at temperatures ranging from 140 to 200 °C. After heating, the solid appears brown to black and consists of nanocrystals that redisperse in chloroform. The nanocrystals are precipitated in excess ethanol to remove residual impurities prior to characterization by transmission electron microscopy (TEM). The yield for the reaction is typically 10 to 20%.

In an alternate preparation, Cu_2S nanodisks are synthesized using tetraoctylammonium bromide (0.18 g $[CH_3(CH_2)_7]_4NBr$ in 25 mL of $CHCl_3$), instead of sodium octanoate, as the phase transfer catalyst. Tetraoctylammonium bromide does not transfer the copper ions to the organic phase as efficiently as sodium octanoate, and the aqueous layer remains blue after stirring for 20 min; however, a sufficient amount of Cu^{2+} ions transfers to successfully produce Cu_2S nanocrystals. Dodecanethiol (240 μL, $C_{12}H_{25}SH$) is added. The mixture is stirred for another 20 min before separating the organic and aqueous phases. Evaporation of the organic solvent gives a waxy solid that serves as the precursor material. Nanocrystals are formed by heating in air with subsequent purification as described above for the nanocrystals synthesized in the presence of octanoate.

The nanocrystals were characterized with transmission electron microscopy (TEM), scanning electron microscopy (SEM), Fourier transform infrared (FTIR) spectroscopy, and differential scanning calorimetry (DSC). High resolution TEM images were obtained using a JEOL 2010F TEM equipped with a field emission gun operating at a 200 kV accelerating voltage. Images were acquired digitally using a Gatan multipole scanning CCD camera with imaging software system. TEM images were also in some cases obtained using a Philips 208 TEM with an 80 kV accelerating voltage. TEM samples were prepared by drop casting nanocrystals dispersed in chloroform onto a 200 mesh carbon coated copper TEM grid purchased from Electron Microscopy Sciences. SEM samples were prepared by drop casting nanocrystals from dispersions on glassy carbon substrates approximately 75 × 75 mm^2 and 1 mm thick. Images were taken on an LEO 1530 SEM equipped with a GEMINI field emission column with a thermal field emitter operating at a 1 kV accelerating voltage. Images were digitally acquired using an Inlens detector and LEO 32 software system. FTIR spectra were obtained on an Infinity Gold (Thermo Mattson, model 960M0019) spectrometer. Samples were prepared by depositing thin films of nanocrystals from solution onto a silicon substrate. Differential scanning calorimetry (DSC) was performed on the copper alkylthiolate precursor deposited in an aluminum sample boat using a Perkin-Elmer DSC 7.

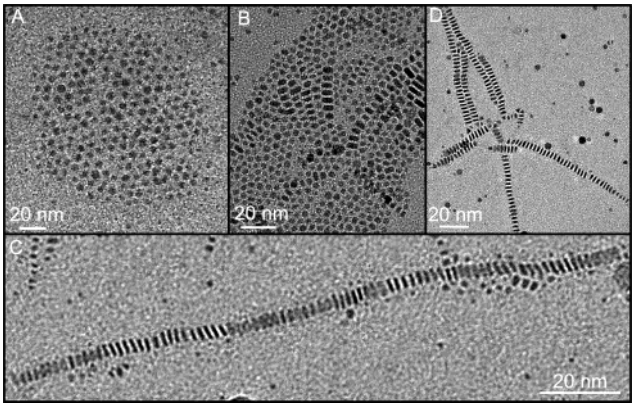

Figure 1. TEM images of Cu_2S nanocrystals and nanoplatelets formed with different reaction times at 155 °C: (A) 30 min, (B) 60 min, (C) 120 min, (D) 150 min.

Results

Synthesis. The reaction temperature and time affect the size and shape of the Cu_2S nanocrystals. The TEM images shown in Figure 1 illustrate how the size and shape evolve with increased reaction time. In Figure 1A−D, TEM images of Cu_2S nanocrystals synthesized at 155 °C reveal the shape evolution from small spherical particles into flat platelets with increased reaction time. After 30 min (Figure 1A), the nanocrystals are small spheres with a 3.2 nm diameter ($\sigma = \pm 19.0\%$ for 400 particles counted). After 60 min (Figure 1B), disklike particles start to form and typically are observed within fields of smaller spheres. The disk diameter increases to 3.6 nm ($\sigma = \pm 21.3\%$ for 400 particles counted). At longer reaction times, the disklike particles tend to stack together into extended chains (Figure 1C and D). The particle size increases to 4.5 nm ($\sigma = \pm 26.6\%$ for 400 particles counted) after 120 min and 5.6 nm ($\sigma = \pm 28.0\%$ for 400 particles counted) after 150 min. Larger disks exhibit increased faceting and orient on the substrate either on end in chains of stacked particles or flat on the substrate. Larger diameter platelets have a higher tendency to lie flat on the substrate relative to smaller disks as seen by the larger isolated particles in Figure 1D.

A high yield of monodisperse nanodisks that self-assemble into chains of stacked disks could be produced over a range of temperatures from 148 to 200 °C (Figure 2). The reaction temperature increases the growth rate but does not qualitatively affect the morphological evolution of the nanocrystals from spheres to nanodisks to faceted nanoplatelets with reaction time. A high yield of nanodisks could be obtained at a range of reaction temperatures by quenching the reaction at shorter times at higher temperatures. Figure 2 shows examples of mono-

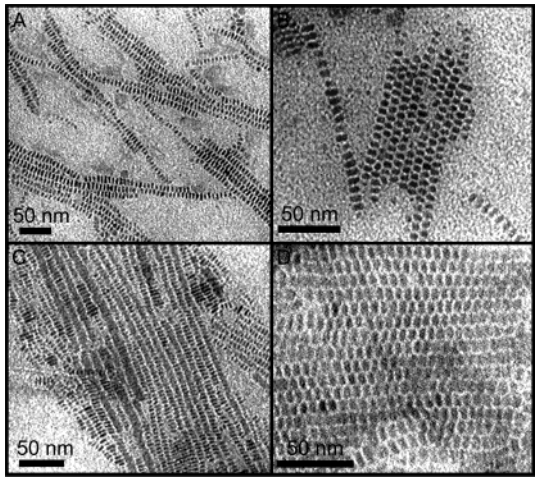

Figure 2. TEM images of self-assembled arrays of Cu_2S nanodisks synthesized at different temperatures and times: (A) 148 °C, 140 min; (B) 165 °C, 90 min; (C) 180 °C, 30 min; (D) 200 °C, 15 min.

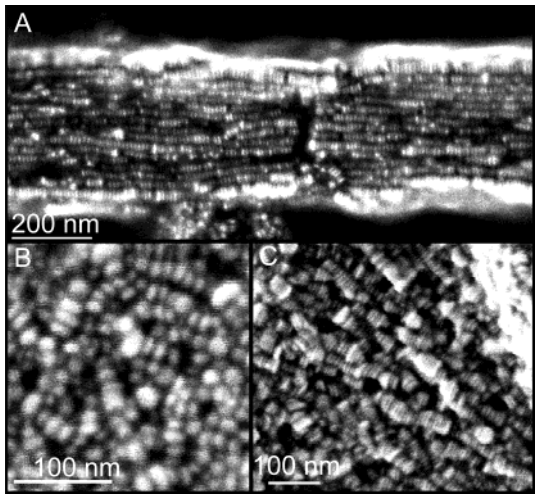

Figure 3. SEM images of self-assembled three-dimensional colloidal crystals of Cu_2S nanodisks formed via deposition of monodisperse (A) and more polydisperse (B) and (C) nanodisks from concentrated dispersions.

disperse nanodisks formed at 148 °C (140 min), 165 °C (90 min), 180 °C (30 min), and 200 °C (15 min). Increased temperature enhances the rate of C−S bond thermolysis of dodecanethiol, which speeds the overall growth rate by increasing S monomer availability to the growing nanocrystals. Increased temperature also increases precursor mass transfer to the nanocrystal surface.

SEM imaging (Figure 3) of nanodisks deposited onto a substrate from concentrated dispersions form 3D colloidal crystals. Monodisperse nanocrystals (Figure 3A) form well-ordered crystals exhibiting parallel alignment of chains of stacked nanodisks with lengths up to a few microns. More polydisperse samples show increased disorder with regard to the spatial registry of the one-dimensional chains of disks forming the colloidal crystal. The long range 1D and 3D ordering observed in these formations appears to result from attraction other than just asymmetric van der Waals attraction. One possibility is that the nanocrystals are ferroelectric as observed in bulk hexagonal Cu_2S with the individual nanocrystal dipole−dipole moments aligning with respect to one another.[17,18]

Disk Morphology. TEM tilting experiments clearly reveal the platelet morphology of the Cu_2S nanocrystals. Figure 4 shows a series of TEM images of a chain of Cu_2S nanodisks stacked side by side taken after horizontal tilting by +15.0°, 0.0°, and −14.7°. The outlined regions highlight disks that appear rodlike when the beam is oriented down the flat axis of the disks and then overlap at off-axis angles. The nanocrystals would not overlap with tilting if they were cylindrical rods because the short axis diameter would not vary with viewing angle. Notice that the apparent overlap between neighboring platelets is large for those with diameters greater than 20 nm but significantly less for those under 20 nm. The sample holder on the JEOL 2010F TEM is constrained to a tilt range of ±15°, which limits the ability to identify the disklike morphology of the nanocrystals as the size decreases. The morphology of particles with diameters smaller than approximately 15 nm is difficult to differentiate by tilt experiments using low resolution TEM, due to the absence of clear overlap between neighboring particles and only minimal change in particle width or interparticle spacing with tilting. However, as discussed below, sample tilting combined with high-resolution TEM imaging of the lattice planes provides an effective way to characterize the nanocrystal morphology.

Crystallographic Orientation of Nanoplatelets. As we reported earlier in ref 16, both high-resolution TEM and XRD reveal that the Cu_2S nanocrystals have the hexagonal (high chalcocite) structure. This is the high-temperature crystal phase of bulk Cu_2S, which undergoes a phase transition at 105 °C from monoclinic (low chalcocite) to hexagonal.[19] The hexagonal structure is thermodynamically favored at the synthetic temperatures and remains metastable in the nanodisks at room temperature. A similar structural metastability has been observed in much larger monoclinic (low chalcocite) Cu_2S nanowires grown at room temperature by flowing H_2S over copper foil.[20] The monoclinic Cu_2S nanowires transform to hexagonal crystal structure when heated above approximately 100 °C.[21] Upon cooling, the nanowires do not structurally relax back to monoclinic until reaching 75 °C. Structural metastability has also been observed in nanocrystals of CdSe[3] and Si[22] below their pressure-induced structural phase transitions, and altogether unique phase behavior in nanostructures is not uncommon, as in the case of Co.[23]

We have performed a detailed analysis of HRTEM images of the Cu_2S nanodisks to determine the crystallographic orientation. Two primary disk orientations on the substrate, disks resting on their side in stacked chains of particles and disks lying flat on the substrate, were studied. Lattice imaging of many particles with different orientations reveals the disks to be single crystals with the [001] direction oriented in the direction of the short axis. Figures 5 and 6 show examples of typical HRTEM images of two disks with different orientations on the substrate.

Figure 5 shows a faceted Cu_2S platelet resting on its face. The 2.0 Å lattice spacing between the {110} lattice planes is

(17) Bieniulis, M. Z.; Corry, C. E.; Hoskins, E. R. *Geophys. Res. Lett.* **1987**, *14*, 135.
(18) Corry, C. E. *Appl. Geophys.* **1994**, *32*, 55.
(19) Buerger, M. J.; Wuensch, B. J. *Science* **1963**, *141*, 276.
(20) Wang, S.; Yang, S.; Dai, Z. R.; Wang, Z. L. *Phys. Chem. Chem. Phys.* **2001**, *3*, 3750.
(21) Wang, S.; Guo, L.; Wen, X.; Yang, S.; Zhao, J.; Liu, J.; Wu, Z. *Mater. Chem. Phys.* **2002**, *75*, 32.
(22) Tolbert, S. H.; Herhold, A. B.; Brus, L. E.; Alivisatos, A. P. *Phys. Rev. Lett.* **1996**, *76*, 4384.
(23) Dinega, D. P.; Bawendi, M. G. *Angew. Chem., Int. Ed.* **1999**, *38*, 1788.

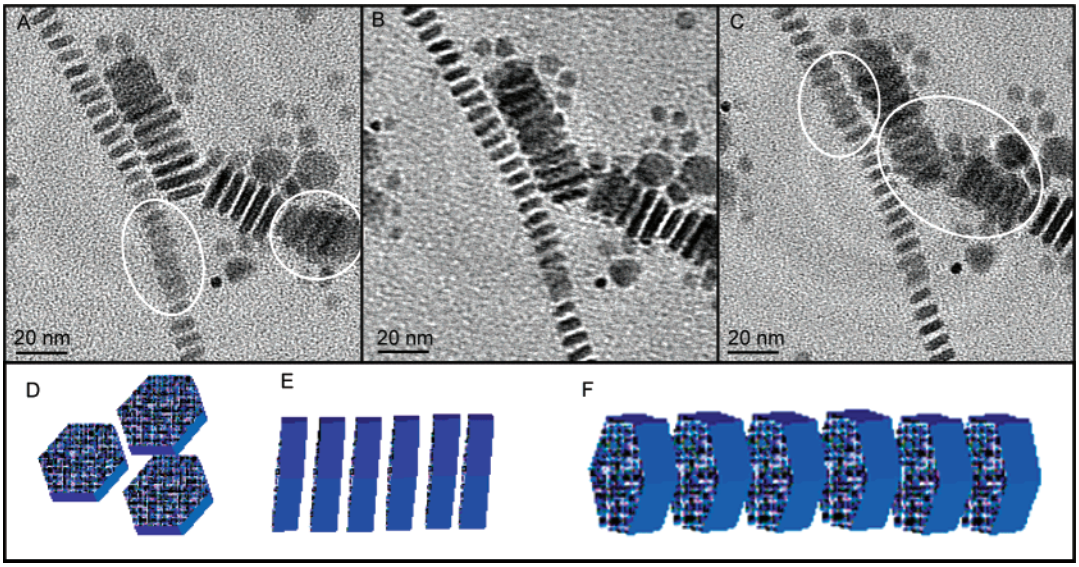

Figure 4. TEM images of stacked nanoplatelets tilted at (A) +15.0°, (B) 0.0°, and (C) −14.7°. The circled regions highlight platelets tilted through the plane of their [001] zone axis. When observing the platelets off-axis, the platelets appear to overlap. Schematic of nanoplatelets oriented (D) parallel to the substrate lying on their major facet, (E) perpendicular to the substrate into a one-dimensional array resembling a rodlike morphology, and (F) tilted with respect to the substrate demonstrating the overlap of each particle when imaged with TEM.

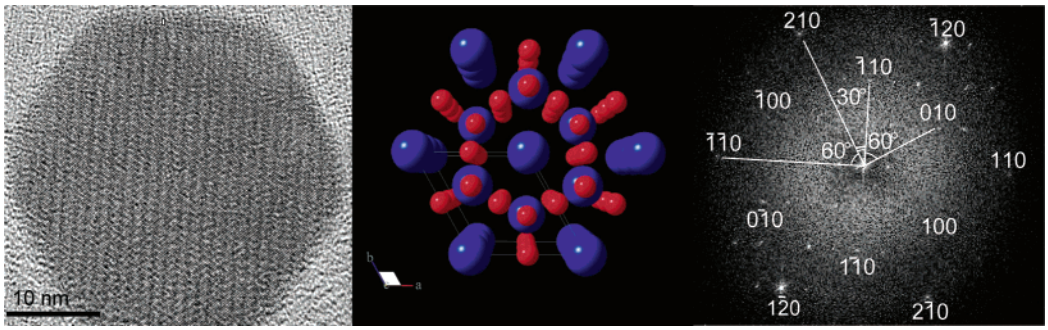

Figure 5. (Left) HRTEM image of a hexagonal platelet lying flat on the substrate with the electron beam incident from the [001] direction. (Middle) Corresponding crystallographic model of the Cu_2S high chalcocite structure when viewed from the same direction as the imaged nanocrystal. (Right) FFT of the imaged nanocrystal demonstrating crystal orientation.

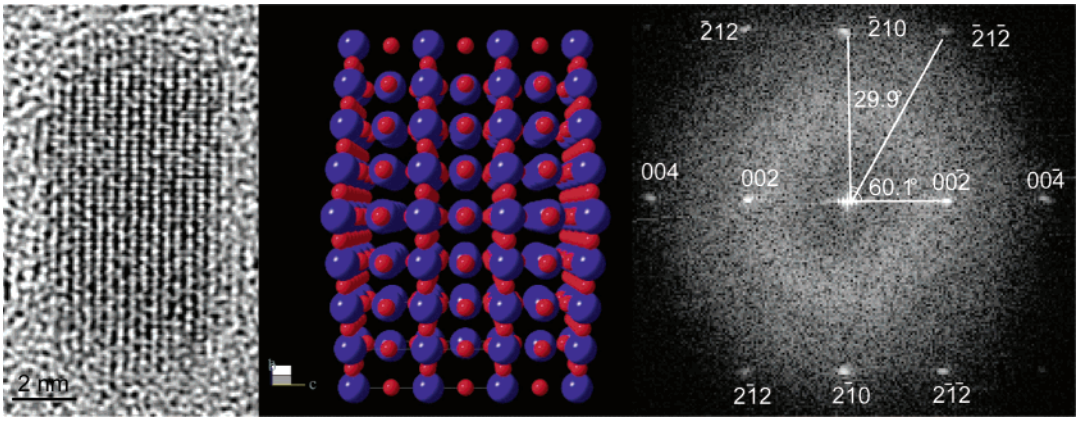

Figure 6. (Left) HRTEM image of a hexagonal platelet standing on end perpendicular to the substrate with the electron beam incident to the [010] direction. (Middle) Corresponding crystallographic model of the hexagonal Cu_2S structure when viewed from the same direction as the imaged nanocrystal showing orientation of the *c*-axis of the crystal in the short growth direction. (Right) FFT of the imaged nanocrystal demonstrating crystal orientation.

visible. The fast Fourier transform (FFT) of the HRTEM image gives a hexagonal array of spots located 3.4 Å from the center spot. These spots are characteristic of the {100} family of planes of hexagonal Cu_2S. The outer hexagonal array of spots located 2.0 Å from the center point corresponds to the {110} family of hexagonal planes. The observed intensities of the {100} reflections are weak compared to the {110} reflections, which is consistent with the selection rules for the hexagonal crystal structure.[24] The 30° rotation of the outer array of spots relative

(24) The minimum intensity, $|F|^2 = f^2$, is expected for the {100} reflections since the Miller indices match $h + 2k = 3m + 1$ and l is even, where F is the structure factor for the unit cell equivalents of the scattering amplitude $f(T)$ and m is an integer. Maximum intensity, $|F|^2 = 4f^2$, is expected for the {110} reflections with Miller indices following $h + 2k = 3m$ and l being even.

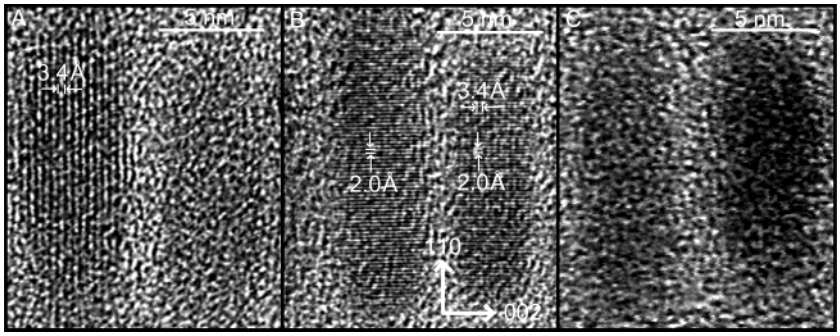

Figure 7. HRTEM images of two nanoplatelets oriented perpendicular to the substrate tilted (A) 0.0° in the *x*- and *y*-directions, (B) −0.6° in the *x*-direction (approximately horizontal to the image) and +6.1° in the *y*-direction (approximately vertical to the image), and (C) an additional 5.4° in the *x*-direction. Images illustrate how the (002) planes (3.4 Å lattice spacing) are oriented perpendicular to the short axis of the nanocrystals with the {110} planes (2.0 Å lattice spacing) oriented parallel. Part C demonstrates how planes are not observed with continued tilting in the *x*-direction.

to the inner array from the {100} planes matches the diffraction pattern expected for an hexagonal lattice with the electron beam incident to the [001] direction.[25] This direction is parallel to the *c*-axis of the Cu_2S crystal structure, indicating that the {001} family of planes is oriented parallel to the substrate in this nanodisk. All of the faceted platelets imaged lying on their face (9 of 9) exhibited this crystallographic orientation.

Figure 6 shows an HRTEM image of a nanoplatelet oriented perpendicular to the substrate. The (002) planes appear to reside parallel to the long axis of the platelet with the (110) planes along the short axis. Analysis of the FFT of the image in Figure 5 helps confirm these assignments. Bright reflections in the FFT corresponding to a 3.4 Å lattice spacing are consistent with the {002} family of planes. These spots are rotated 90° relative to the {110} reflections with a lattice spacing of 2.0 Å. The reflections corresponding to the {112} family of planes complete the rectangular array of spots with a lattice spacing of 1.7 Å. These reflections are 29.9° from the {110} reflections and 60.1° from the {002} reflections. The reflections for the hexagonal {001} and {003} planes are forbidden and do not appear in the FFT pattern. The FFT corresponds to the standard indexed diffraction pattern of an hexagonal crystal with the incident electron beam oriented in the [010] direction except for two deviations.[25] First, the angles between the {112} reflections and the {002} and {110} reflections are 57.8° and 32.2° for the standard diffraction pattern of a hexagonal crystal. This corresponds to a 2.3° shift from the standard pattern. Second, the ratios of lengths between the (−212) and (002) and the (−210) and (002) reflections are larger for the Cu_2S pattern than the standard hexagonal pattern. These variations result from the slight elongation of the *c*-axis observed in the Cu_2S high chalcocite crystal structure. A determination of the angles between these planes for the high chalcocite structure matches exactly the measured values from the FFT. The incident electron beam is oriented perpendicular to the *c*-axis, exactly 90° relative to the direction of the beam used to image the platelet in Figure 5. The FFT of the Cu_2S nanodisk in Figure 6 confirms that the (002) planes reside parallel to the long axis of the platelet with the (110) planes along the short axis. Again, the *c*-axis of the hexagonal crystal structure is parallel to the short growth direction of the platelet.

The majority of nanodisks imaged on their side, such as the one in Figure 6, reveal a crystallographic orientation rotated exactly 90° from platelets lying on their face. A cylindrical rod would not exhibit a preferred lattice orientation in the tilt experiments. The fact that the (002) lattice planes of nanocrystals with diameters smaller than 15 nm are normal to the slow growth direction of stacked particles provides evidence of platelet morphology; however, HRTEM can provide more conclusive evidence by determining if the [010] zone axis is within the tilt range of the sample holder (±15°) for the majority of nanocrystals. When the beam is oriented down the [010] zone axis, both the (002) and (110) planes become visible. Figure 7 shows HRTEM images of two nanodisks at three different tilt angles. In Figure 7A, the (002) lattice fringes are visible along the long axis of the particle on the left. After tilting the sample −0.6° in the *x*-direction (approximately horizontal to the image) and +6.1° in the *y*-direction (approximately vertical to the image) (Figure 7B), the particle on the left reveals the (110) fringes parallel to the short axis and the particle on the right exhibits both the (002) fringes along the long axis and the (110) fringes along the short axis. Tilting an additional −5.4° in the *x*-direction eliminates the lattice fringes. A small variation in tilt angle of only a few degrees was necessary to find the [010] zone axis in each particle. The preferential alignment of the [010] direction orthogonal to the substrate provides confirmation that the smaller rodlike particles are indeed nanodisks.

Visualization of the hexagonal Cu_2S crystal structure using the "Balls and Sticks" software package helps illustrate the relationship between the crystallographic orientation and the favored growth direction of the nanodisks. The high chalcocite structure has the $P6_3/mmc$ space group with a primitive hexagonal unit cell, $a = 3.89$ Å and $c = 6.88$ Å. Buerger and Wuensch modeled the XRD patterns of bulk high chalcocite and determined the location of S atoms at the hexagonal sites (S′ at 0 0 0 and S″ at 0.333 0.667 0.25). The Cu atoms are located at a fraction of three interstitial locations (Cu′ in 2b at 0 0 0.25, Cu″ in 4f at 0.333 0.667 0.578, Cu‴ in 6g at 0 0.5 0).[19] Each primitive hexagonal cell contains four S atoms and eight Cu atoms with each Cu atom having a total of 12 lattice locations which they occupy at a ratio of 1.24:1.63:1.13 for each of the three possible groups of sites.[19] The Cu atoms in high chalcocite have been described as being disordered with rapid diffusion between possible interstitial locations.[26,27] The atomic models in Figures 5 and 6 showing the Cu and S atoms as viewed from the [001] and [010] directions, respectively, are

(25) Williams, D. B.; Carter, C. B. *Transmission Electron Microscopy: A Textbook for Materials Science*; Plenum Press: New York, 1996.

(26) Buerger, M. J. *Anais Acad. Brasil. Cienc.* **1949**, *21*, 261.
(27) Jensen, M. L. Ph.D. Thesis, Massachusetts Institute of Technology, 1951.

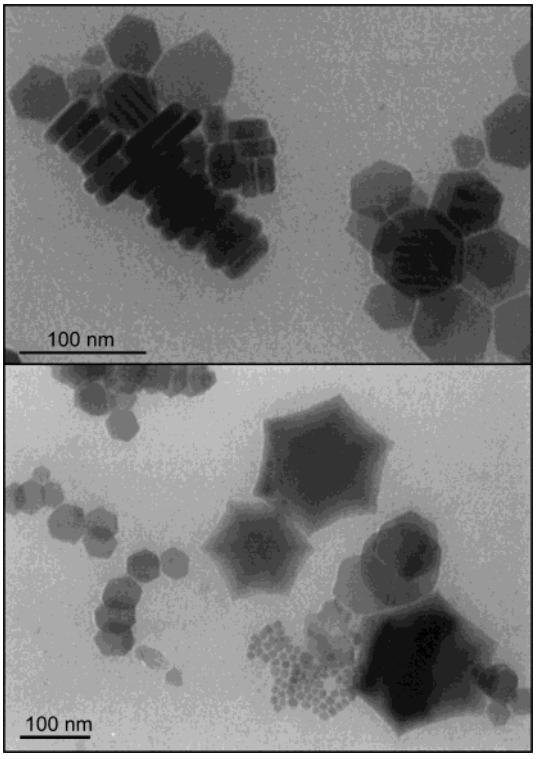

Figure 8. TEM images of typical Cu_2S nanocrystals formed by replacing sodium octanoate with tetraoctylammonium bromide as the phase transfer catalyst.

consistent with the measured FFT patterns. Therefore, the faceted disk morphology results from growth favored in the ⟨100⟩ directions.

Reaction Mechanism and Role of Capping Ligand. A mixture of octanoate and dodecanethiol is used to synthesize the Cu_2S nanodisks. Clearly, dodecanethiol provides the sulfur source to the growing nanocrystals; however, what role does dodecanethiol play in terms of controlling particle growth? Octanoate serves as the phase transfer catalyst to solubilize copper cations in the organic solvent, but what role does octanoate play during the synthesis? As discussed below, we found with the aid of FTIR spectroscopy that octanoate serves as the primary capping ligand that controls nanocrystal growth with dodecanethiol providing little steric stabilization.

When tetraoctylammonium bromide (TOAB) was used in place of sodium octanoate as the phase transfer catalyst, the Cu_2S nanodisks exhibited the same morphology, but the disk size was much larger, as shown in Figure 8. In addition, the disks exhibited less "rounding" of the crystal facets, and in some cases, accelerated ⟨110⟩ growth with respect to the {100} crystal facets appears to have given rise to convex curvature of the platelet facets. These disks exhibited the high chalcocite Cu_2S crystal structure, which was verified by indexing FFT patterns of HRTEM images with lattice resolution.

Figure 9 compares FTIR spectra for pure sodium octanoate, and nanocrystals synthesized in the presence of sodium octanoate and tetraoctylammonium bromide (TOAB). The characteristic methyl and methylene stretches appear at 2962, 2924, 2872, and 2853 cm^{-1} in the FTIR spectra of octanoate, octanoate-capped nanodisks, and disks synthesized with TOAB. The FTIR spectra in Figure 9A and B both exhibit bands at 1570 and 1710 cm^{-1} characteristic of C−O stretching in the

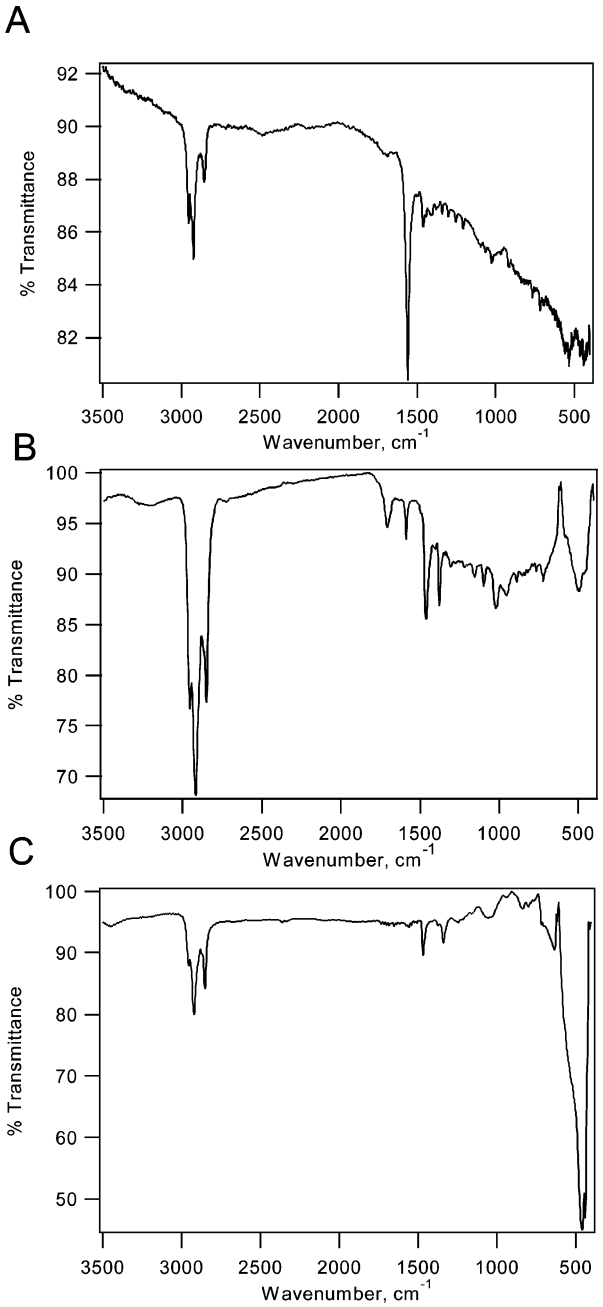

Figure 9. FTIR spectra of (A) sodium octanoate, (B) Cu_2S nanocrystals formed with sodium octanoate as the phase transfer catalyst, and (C) Cu_2S nanocrystals formed with tetraoctylammonium bromide as the phase transfer catalyst.

carboxylate ion and prominent bands at 1378 and 1463 cm^{-1} corresponding to C−H bending frequencies. Nanodisks formed without sodium octanoate do not have absorption bands at 1570 and 1710 cm^{-1}. The TOAB-synthesized nanodisks did show prominent C−H bond bending bands at 1342 and 1469 cm^{-1} with a small peak at 1378 cm^{-1} that match those of both neat 98% 1-dodecanethiol and TOAB.[28] The nanodisks synthesized in the presence of TOAB are coated with either dodecanethiol, TOAB, or a combination of the two as the capping ligand. Regardless of the actual ligand capping these nanocrystals, ligand adsorption on the particles is significantly weaker for

(28) Pouchert, C. J., Ed. *The Aldrich Library of FT-IR Spectra*, 2nd ed.; Sigma-Aldrich: Milwaukee, WI, 1997; Vol. 1.

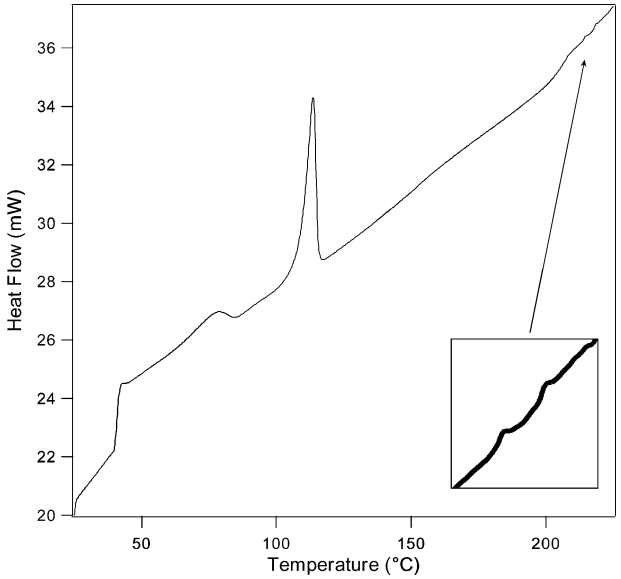

Figure 10. DSC curve for heating the initially unreacted copper thiolate precursor from 25 to 225 °C.

dodecanethiol and TOAB compared to octanoate, based on the larger particle size obtained with TOAB under reaction conditions similar to the octanoate-controlled reactions.

The temperature dependence of the copper alkylthiolate precursor decomposition was examined by DSC. Figure 10 shows a DSC scan of the precursor heated from 25 °C to 225 °C. A broad peak appears at temperatures ranging from 43 °C to 78 °C due to the melting of the precursor from its initial waxy state to a viscous fluid. The sharp peak at 113.5 °C results from the decomposition of the copper alkylthiolate precursor as the C−S bond is cleaved to form Cu_2S. Two small peaks shown in the inset of Figure 10 at 214.5 and 218.5 °C correspond to the slightly elevated boiling points for 1-dodecene and dodecane (normal bp of 213 and 216 °C) confirming that the dodecanethiol C−S bond is cleaved and no further decomposition of the organic chain occurs.

Discussion

The octanoate serves as the capping ligand that stabilizes nanodisk size and shape. This is consistent with observed chemisorption of alkylated carboxylic acids on Cu (100) surfaces.[29] Although dodecanethiol and/or TOAB can serve to a limited extent as a capping ligand, as confirmed by FTIR of nanodisks synthesized using TOAB, C−S bond cleavage is what gives rise to particle growth and therefore cannot serve as a chemically inert passivant. Octanoate slows particle growth by reducing monomer accessibility to the particle surface. The nanocrystal morphology, however, appears to be independent of the chemical nature of the capping ligand, which is different than CdSe and Co where the capping ligand chemistry is critical to nanodisk and nanorod formation.[2,3]

In the thermodynamic limit, the face-dependent surface energies dictate particle shape and faceting. Matysina determined that hexagonal metals with c/a ratios greater than the ideal hexagonal values (i.e., c/a > 1.633) have (101) and (100) surface energies approximately 1.5 times larger than those for the (001) facets.[30] Hexagonal Cu_2S has a c/a ratio of 1.697 and should

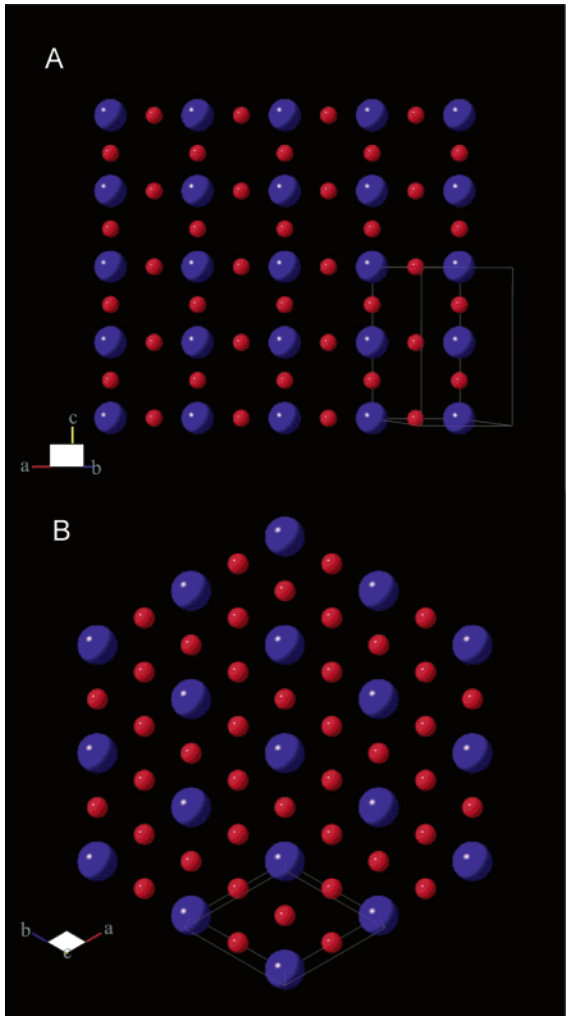

Figure 11. Crystallographic model showing the most atomically dense layers of atoms for the {100} planes (A) and {001} planes (B) of the hexagonal Cu_2S structure.

exhibit higher surface energies on the (101) and (100) lattice planes. The formation of large (001) crystal facets limits exposure of these higher energy surfaces but, to an extent, much greater than expected from these thermodynamic considerations. In other words, nanodisk growth is more anisotropic than expected based on surface energy considerations: for example, the surface-to-volume ratio is 0.49 for a hexagonal platelet with sides 15 nm long and a 6 nm thickness versus 0.26 for a sphere of equivalent total volume. Likewise, the growth of hexagonal prisms does not resemble expectations for rapid, kinetically controlled growth similar to what occurs along the *c*-axis in monoclinic Cu_2S nanowires or CdSe nanorods.[3,21]

The reaction kinetics of dodecanethiol thermolysis appear to largely determine the nanodisk shape. Pure dodecanethiol (boiling point is 266 to 283 °C) is chemically stable over all the reaction temperatures examined yet provides S monomer through C−S bond thermolysis. Kühnle et al. and Vollmer et al. investigated dodecanethiol adsorption on Cu(110) and Cu(100) surfaces and found that the C−S bond cleaves at temperatures greater than 127 °C to form monolayers of adsorbed sulfur.[31,32] Laibinis et al. detected increased S con-

(29) Dubois, L. H.; Zegarski, B. R.; Nuzzo, R. G. *Langmuir* **1986**, *2*, 412.
(30) Matysina, Z. A. *Mater. Chem. Phys.* **1999**, *60*, 70.
(31) Kuhnle, A.; Vollmer, S.; Linderoth, T. R.; Witte, G.; Woll, C.; Besenbacher, F. *Langmuir* **2002**, *18*, 5558.
(32) Vollmer, S.; Witte, G.; Woll, C. *Langmuir* **2001**, *17*, 7560.

centrations on Cu thin films after exposure to alkanethiols of varying chain lengths in isooctane solutions, indicating the formation of thin layers of Cu_2S at the Cu film interface.[33]

Studies of alkanethiol adsorption on Cu(111) surfaces revealed that the outermost Cu atomic layers reconstruct into a pseudo-(100) layer.[34−36] Thiolate adsorption on Cu(110) and Cu(100) surfaces does not give rise to a surface reconstruction.[31,32] Apparently, the Cu(111) surface reconstructs because thiol adsorption on the Cu(100) surface is much more energetically favorable and actually reorients the (111) planes.[35] On the pseudo-(100) plane, the S atoms lie on the 4-fold hollow sites located between Cu atoms with a lateral expansion of 3.5% × 15% with respect to a true Cu (100) lattice plane.[35] This surface reconstruction is consistent with the tendency of sulfur to form chemically stable 4-fold coordination with Cu.[37,38] Interestingly, the copper atoms in the {100} planes of Cu_2S exhibit a square lattice with sites available for 4-fold coordination to adsorbed sulfur (Figure 11A). In fact, the Cu sublattice is expanded enough to accommodate S atoms within the lattice plane. The {001} planes do not exhibit this 4-fold symmetry. Based on the crystallographic orientation of the nanodisks, the Cu_2S preferentially grows in the ⟨100⟩ directions as opposed to the ⟨001⟩. This growth direction provides faces with the 4-fold surface sites that promote S adsorption and incorporation to form the next layer of Cu_2S. In comparison, the {001} planes (Figure 11B) are the most atomically dense structures with S atoms lying in 6-fold sites and are expected to kinetically inhibit S addition.

Summary

In the solventless Cu_2S nanodisk synthesis, sodium octanoate functions as both the phase transfer catalyst and the capping ligand. The hexagonal (high chalcocite) nanodisks are faceted platelets with the *c*-axis oriented perpendicular to the faster growing {100} planes. Nanodisk growth is limited in the [001] direction and predominantly occurs along the six energetically equivalent {100} directions to form hexagonal prisms. The nanodisk shape appears to relate to the preferred adsorption and cleavage of dodecanethiol on {100} facets compared to the {001} facets as expected based on alkanethiol adsorption studies demonstrating preferential S adsorption at 4-fold coordinating Cu surface sites. Anisotropic control of crystal morphology based on face-sensitive surface reactivity offers an interesting potential avenue for controlling nanostructures with different shape.

Acknowledgment. We thank D. Jurbergs and F. Mikulec for valuable discussions. We also thank the National Science Foundation, the Welch Foundation, and the Texas Higher Education Coordinating Board through its ATP program for financial support.

JA037688A

(33) Laibinis, P. E.; Whitesides, G. M.; Allara, D. L.; Tao, Y.-T.; Parikh, A. N.; Nuzzo, R. G. *J. Am. Chem. Soc.* **1991**, *113*, 7152.
(34) Imanishi, A.; Isawa, K.; Matsui, F.; Tsuduki, T.; Yokoyama, T.; Kondoh, H.; Kitajima, Y.; Ohta, T. *Surf. Sci.* **1998**, *407*, 282.
(35) Driver, S. M.; Woodruff, D. P. *Surf. Sci.* **2001**, *479*, 1.
(36) Driver, S. M.; Woodruff, D. P. *Langmuir* **2000**, *16*, 6693.
(37) Foss, M.; Feidenhans'l, R.; Nielsen, M.; Findeisen, E.; Buslaps, T.; Johnson, R. L.; Besenbacher, F. *Surf. Sci.* **1997**, *388*, 5.
(38) Jackson, G. J.; Driver, S. M.; Woodruff, D. P.; Cowie, B. C. C.; Jones, R. G. *Surf. Sci.* **2000**, *453*, 183.